Flexible Thermoelectric Electrodes of the New Nitrogen-Modified Mxene/SWCNT Layered Structure Used For Low-Grade Thermal Energy Collection

Shang Hai,
China
LightorEther@outlook.com;

Abstract - Confronting the global challenge of energy efficiency in the backdrop of environmental concerns, the innovation of flexible thermoelectric electrodes marks a significant stride forward, especially in the realm of low-temperature heat recovery. This investigation unveils a pioneering electrode material, a nitrogen-doped SWCNT/MXene bilayer thin film, meticulously engineered for thermoelectric systems. Surpassing the conventional Pt electrodes, which are often hindered by their inherent inflexibility and prohibitive costs, our proposed electrodes have excellent ductility and good thermoelectric properties. At a modest temperature difference of 40°C, the thermopower output reaches 14.11µW cm^{-2} and the Seebeck coefficient rises to 1.61mV K^{-1}, significantly improving the thermoelectric performance significantly. This innovation not only positions itself as a formidable contender to Pt electrodes but also signals a new dawn for efficient thermoelectric energy harvesting, underscored by the material's scalability and ready availability.

Keywords: Flexible Thermoelectrics, Heat Recovery, Nitrogen-Modified, Energy Sustainability

1. Introduction

Confronting the escalating global energy crisis, the strategic harnessing of low-grade thermal energy has surfaced as a pivotal solution in advancing sustainable energy practices[1]. Defined as thermal energy available at relatively modest temperatures, typically below 120°C, low-grade heat represents an extensively underutilized resource[2]. This type of heat, frequently discarded as waste by industrial processes, natural geothermal activities, and routine human endeavors, holds immense potential for bolstering energy efficiency and diminishing reliance on fossil fuels, thereby reducing environmental impacts. In an era marked by growing energy demands, the sustainable procurement and transformation of low-grade thermal energy into functional electricity is indispensable, particularly given the widespread prevalence of such heat sources[3].

At the vanguard of this venture is the technological evolution of Thermoelectric Converters (TECs), lauded for their proficiency in transducing heat directly into electrical energy via the Seebeck effect[4]. TECs have emerged as a paradigm shift in energy harvesting, especially in the context of low-grade heat, attributed to their solid-state design, absence of mechanical components, and versatile operation across diverse temperature gradients. Central to the effectiveness of TECs is the innovation and development of efficient and reliable electrodes[5]. The performance of these electrodes is paramount in defining the overall efficacy of TECs, directly impacting key parameters such as the Seebeck coefficient, electrical conductivity, and thermal conductivity. These fundamental properties dictate the extent of electricity generation from thermal energy[6]. Recent advances in electrode material science have been oriented toward not only amplifying these thermoelectric attributes but also ensuring the electrodes' adaptability to a multitude of thermal environments and practical scenarios[7]. The progressive enhancement of TEC electrodes, particularly through the integration of novel materials, underscores the commitment to refining thermoelectric energy conversion and the efficient harnessing of low-grade thermal energy.

In this context, the exploration of MXene[8] and single-walled carbon nanotubes (SWCNTs)[9] as cutting-edge materials for thermoelectric battery electrodes has captured considerable scientific interest. MXene, distinguished by their exceptional electrical conductivity and customizable surface chemistry, are posited as significantly augmenting the efficiency of thermoelectric batteries. Their stratified architecture promotes superior electron mobility, pivotal in optimizing electrode attributes like the Seebeck coefficient and electrical conductivity[10]. The inherent flexibility of MXene renders them especially apt for fabricating electrodes in next-generation thermoelectric batteries, accommodating diverse surface geometries and dynamic operational conditions[11].

Complementing MXene, SWCNTs, with their distinctive one-dimensional nanostructure and remarkable physicochemical traits, bring a synergistic set of qualities essential for thermoelectric battery electrodes[12]. Their notable electrical conductivity coupled with low thermal conductivity is crucial for sustaining temperature differentials vital for effective energy conversion in thermoelectric batteries[13]. Additionally, the pliability and mechanical resilience of SWCNTs earmark them as ideal for the creation of adaptable and robust electrodes[14].

The integration of MXene and single-walled carbon nanotubes (SWCNTs) in thermoelectric batteries, particularly within electrode technology, faces considerable challenges, despite their inherent potential[15]. The primary challenge involves achieving an optimal synergy between SWCNTs' notable electron mobility and MXene's structural benefits[16]. This synergy is crucial for developing a composite electrode material that not only excels in thermoelectric performance but also maintains the essential flexibility for a broad spectrum of applications.

A significant issue in this integration is the dissimilar nature of MXene and SWCNTs, which often leads to problems with uniform dispersion and interfacial compatibility[17]. MXenes, characterized by their two-dimensional layered structure, provide excellent electrical conductivity and a base for functionalization[11]. However, integrating them with one-dimensional SWCNTs, renowned for exceptional electron mobility and mechanical strength, requires a sophisticated approach to maintain these properties while mitigating issues such as aggregation and poor interfacial bonding[18]. To navigate these challenges, innovative strategies, including surface functionalization, chemical modification, and advanced fabrication techniques, have been explored. Surface functionalization aims to enhance MXene and SWCNT compatibility, fostering a more uniform mixture and improved electron transfer across interfaces[19]. Chemical modifications, like doping or creating controlled defects, are employed to fine-tune the composite's electronic attributes, achieving an optimal balance between electrical conductivity and thermopower[20]. Moreover, advanced fabrication techniques that enable precise control over the composite's microstructure are crucial[21]. Methods such as layer-by-layer assembly, electrospinning, or meticulous vacuum filtration are employed to create well-structured MXene/SWCNT architectures. These techniques facilitate a cohesive network where MXenes and SWCNTs are intimately integrated, ensuring efficient charge transfer while simultaneously reducing thermal conductivity due to phonon scattering at interfaces[22].

Overcoming these hurdles allows the MXene/SWCNT composite electrodes to realize the desired synergy, where MXene's structural stability and electrical conductivity are complemented by SWCNTs' high electron mobility and mechanical resilience[23]. This harmonious integration is anticipated to catalyze significant advancements in thermoelectric batteries, leading to high energy conversion efficiency, enhanced durability, and the versatility required for diverse practical applications[24].

In this study, we introduced a cutting-edge nitrogen-modified SWCNT and MXene bilayer thin film (MS-N), meticulously crafted for thermoelectric battery electrodes. Alongside, we conducted a comprehensive comparative analysis, juxtaposing the MS-N electrode with its counterparts: the MXene and single-walled carbon nanotubes (SWCNT) bilayer thin film (MS), the MXene-SWCNT mixed thin film (M+S), and the conventional platinum electrode[25-28].This comparison robustly affirmed the MS-N electrode's feasibility and enhanced performance, underlining its superiority over both the traditional metal electrodes and other composite configurations[29]. The MS-N's bilayer structure seamlessly melds MXene and SWCNT, offering an efficient electron transport and thermal management pathway. This layered approach leverages SWCNTs' high electron mobility and MXene's structural stability and electrical conductivity, elevating the composite beyond the realm of traditional monolithic thermoelectric materials. It strikes an essential balance, optimizing electrical conductivity and the Seebeck coefficient while reducing thermal conductivity – key to maximizing thermoelectric efficiency. Furthering this structural innovation, the nitrogen modification substantially enhances the MS-N composite's performance. It meticulously refines the electronic structure, bolsters chemical reactivity, and introduces sophisticated surface functionalities, cumulatively heightening the low-temperature thermoelectric conversion efficiency. This nitrogen modification advances the material interface, boosting carrier concentration and diminishing the energy barrier for electron transport, thus augmenting the MS-N material's overall thermoelectric attributes. This holistic strategy, integrating the bilayer structure with nitrogen modification, positions the MS-N composite as a strong competitor in the thermoelectric battery domain. It emerges as a robust

alternative to traditional electrode materials, forging new avenues in efficient and sustainable energy conversion technologies. The MS-N's scalability and cost-effectiveness highlight its potential for broad-based applications, signifying a signifying a pivotal advancement in utilizing low-grade thermal energy in both commercial and environmental settings. The The dual emphasis on structural and chemical optimization in MS-N electrodes redefines the standards in thermoelectric material design, heralding the creation of more efficient and versatile thermoelectric devices (Fig.1).

2. Experimental section

2.1. Materials and reagents

Single-Walled Carbon Nanotubes (SWCNTs), Potassium Chloride, Lithium Fluoride, Hydrochloric Acid, Potassium Ferricyanide, Potassium Ferrocyanide, Polyvinylpyrrolidone (PVP), Titanium Aluminum Carbide (Ti_3AlC_2), Ethanol, all of the above from Sigma-Aldrich or Adamas. All water used for solution preparation is deionised water.

2.2. Apparatus

The microscopic morphology of the samples was observed using a Hitachi S-4800 Scanning Electron Microscope (SEM). The crystal structure of the samples was analyzed using X-ray Diffraction (XRD) with a Bruker D8-Advance X-ray diffractometer (Germany), setting the scanning range from 5° to 80°. Raman spectroscopy was conducted using the SENTERRA (China) from Bruker Optics. X-ray Photoelectron Spectroscopy (XPS) measurements were carried out using a Thermo Scientific K-Alpha (USA). Nitrogen isothermal adsorption and desorption curves (BET) were performed using a Quantachrome Nova 4000e (USA).

All electrochemical tests were conducted in a solution of 0.1 M KCl and 5 mM $[Fe(CN)_6]^{3-/4-}$, unless otherwise specified. All electrochemical experiments were carried out at room temperature using a conventional three-electrode system. The three-electrode system consisted of a saturated silver chloride electrode as the reference electrode and a platinum electrode as the counter electrode. The electrochemical instrument used was the CHI 760E electrochemical workstation from CH Instruments, China. For Cyclic Voltammetry (CV) tests, a scan rate of 0.1 V/s was selected unless otherwise specified. Electrochemical Impedance Spectroscopy (EIS) tests were conducted with frequency parameters set from 0.01 Hz to 100 kHz.

2.3. Preparation of SWCNT Aqueous Dispersion and Etching of MXene Materials

To prepare the SWCNT aqueous dispersion, 1g of SWCNT powder was initially used, to which 50mg of PVP powder was added to aid in the dispersion of the carbon nanotubes and assist in film formation. This mixture was then combined with 100mL of deionized water. The solution was stirred using magnetic stirring equipment at room temperature for 2 hours, yielding a 10 mg/mL single-walled carbon nanotube aqueous dispersion.

$Ti_3C_2T_x$ was synthesized through a conventional etching process using the MAX-phase precursor Ti_3AlC_2. Initially, 2 g of NaF powder was incrementally added to a mixture comprising 20 mL of 12 M HCl and 20 mL of deionized water. Subsequently, 2 g of Ti_3AlC_2 was gradually introduced into this mixture. The ensuing reaction was maintained under continuous stirring at 60 °C for a duration of 48 hours. Following this, the resultant suspension underwent centrifugation, filtration, and multiple washes with deionized water until the pH of the filtrate reached approximately 6. Finally, the $Ti_3C_2T_x$ was vacuum-dried at 70 °C.

2.4. Preparation of M+S, MS and MS-N electrodes

For the fabrication of M+S electrode films, an initial mixture was prepared by combining 2 mL of SWCNT aqueous dispersion with etched MXene powder, followed by the addition of 13 mL of deionized water. This mixture was then subjected to homogenization using a magnetic stirrer for a duration of 24 hours. Subsequently, the resultant solution was processed through a recirculating water vacuum filtration apparatus to form films. The M+S electrode films were synthesized in varying compositions by altering the mass of MXene powder used (10 mg, 20 mg, 30 mg, 40 mg), resulting in films designated as 20S+10M, 20S+20M, 20S+30M, and 20S+40M, respectively.

In the preparation of MS electrode films, 20 mg of etched MXene powder was mixed with 10 mL of deionized water and stirred for 2 hours using a magnetic stirrer to create an MXene aqueous dispersion. Initially, a layer of SWCNT film was

formed by vacuum filtration of 2 mL of SWCNT aqueous dispersion, upon which the prepared MXene dispersion was directly applied and filtered, resulting in the formation of the MS electrode film.

All the electrode films were subjected to vacuum drying at 60°C to remove residual moisture. The dried films were cut into 1 cm^2 electrode squares for subsequent testing. To prepare the MS-N electrodes, the dried MS films were placed a tube furnace under a continuous nitrogen flow and heated at 200°C for 2 hours.

3. Results and discussion
3.1. Characterization of materials

The morphological features of $Ti_3C_2T_x$ and MS-N thin film electrodes were explored using Scanning Electron Microscopy (SEM). Fig.2a showcases the morphology of 2D exfoliated $Ti_3C_2T_x$ obtained through selective etching of the MAX phase from Al metal, exhibiting a compact and well-aligned multilayer $Ti_3C_2T_x$ typical of two-dimensional layered structures, conducive to enhanced electrical conductivity. The MXene facets, even after a simple vacuum-assisted filtration method followed by nitrogen modification, retained the characteristic layered structure of multilayer $Ti_3C_2T_x$ as depicted in Fig.2b. The SWCNT networks, composed of long and flexible clusters of carbon nanotubes throughout the SWCNT film, exhibited no significant defects or material loss(Fig.2c)[30]. The chemical bond changes in MS-N flexible electrode films before and after annealing were studied in depth using Raman spectroscopy. The full Raman spectrum illustrated in Fig.2d reveals the typical peaks of SWCNT, including the D band at 1340 cm^{-1}, the G band at 1570 cm^{-1}, and the G$^+$ band at 1590 cm^{-1}[31]. The intensity ratio of the G+ band to the D band (G/D ratio), indicative of the film's defect level, was thus normalized as shown in Fig.2f to clearly reflect the G/D ratio, with a higher intensity of the D band corresponding to a lower G/D ratio. It was evident that the G/D ratio of the MS-N film annealed in N^2 was lower than that of the fabricated MS film, suggesting that N^2 modification introduced more defects due to the lower G/D ratio indicating a higher degree of defects[32].

Furthermore, X-ray Photoelectron Spectroscopy (XPS) was utilized to elucidate the chemical states and bonding information of the MS-N film. The Ti 2p spectrum of the MXene facet (Fig.2g) displayed several peaks located at $\approx$ 455.1, $\approx$ 457.8, $\approx$ 458.6, and $\approx$ 461.9 eV, corresponding to Ti-C, Ti-OH, Ti-O, and TiO$_2$, respectively[33]. The prominence of Ti-OH indicated partial oxidation of the film surface along with the presence of hydroxyl functional groups. The presence of hydroxyl groups enhances the material's hydrophilicity, which is beneficial for the absorption of electrolytes and the facilitation of redox reactions. The oxidized state of Ti-O is crucial for improving the material's stability and electrochemical performance[34]. The C 1s spectrum of the SWCNT facet (Fig.2h) was divided into three peaks at 284.8 eV, 285.3 eV, and 287.5 eV, corresponding to C-C (sp^2), C-C (sp^3), and N-C (sp^2) bonds, respectively; the formation of N-C bonds effectively confirmed the efficacy of N^2 modification. Fig.2i presents the complete XPS curves of the MXene and SWCNT facets of the MS-N film, thoroughly revealing the elemental composition of the film.

3.2. Electrochemical studies

In the cyclic voltammetry (CV) analysis conducted within a 0.1 M potassium chloride and 5 mM $[Fe(CN)_6]^{3-/4-}$ electrolyte, a comparative study of four distinct electrode types was undertaken: Fig.3a show the conventional metal electrode Pt, a MXene and SWCNT composite electrode (M+S), a layered MXene and SWCNT electrode (MS), and a nitrogen-annealed MXene/SWCNT layered electrode (MS-N). The CV assessments revealed a notably larger electrochemical activity area for the layered electrodes (MS and MS-N) in comparison to both the M+S composite and the traditional Pt electrode, underscoring the enhanced electrochemical reactivity of the layered configurations. Particularly, the MS-N electrode exhibited a larger CV area than its unmodified MS counterpart, confirming the efficacy of the nitrogen annealing modification. Fig.3b shows that the peak redox current of MS-N increases with scanning velocity from 5 to 50 mV/s, showing a good linear relationship with scanning velocity, indicating that the process is reversible surface sorption driven. (Fig.3b-c)

Subsequent Electrochemical Impedance Spectroscopy (EIS) evaluations of the modified electrodes indicated a significant refinement in interfacial properties (Fig.3d). The semicircle diameter in the high-frequency region of the EIS spectrum, indicative of the charge transfer resistance (Rct), reflected the electron transfer dynamics at the

nanocomposite material-electrode interface, was found to be 1.86Ω. The Equivalent Series Resistance (ESR) intersecting the real axis at high frequencies, signified the cumulative internal resistance from the electrolyte, e lectrode materials, and interface contacts, was found to be 14.04Ω. A notable reduction in both Rct and ESR was observed for the MS and MS-N electrodes compared to the Pt and M+S electrodes. Furthermore, the linear response in the low-frequency domain, attributed to diffusion-controlled electrode processes, highlights the significant impact of material diffusion within the electrolyte. Collectively, these findings not only underscore the superior electrochemical performance of the MS-N electrode but also emphasize its potential as a highly efficient thermoelectric material.

3.3. Electrochemical studies

In this study, the thermoelectrochemical Seebeck coefficient (Se) of Thermoelectric Converters (TECs) was meticulously measured using a bespoke experimental setup comprising a pair of electrolytic cells adjoined by a salt bridge. This arrangement was instrumental in engendering a stable and precisely controllable thermal gradient between the cells, thereby cultivating an optimal experimental milieu for the quantification of Se. The experimental apparatus was meticulously calibrated, with each electrolytic cell being encased within a circulatory water system. This setup enabled the precise modulation of temperatures, whereby one cell functioned as a 'hot anode' at a higher temperature, and the other served as a 'cold cathode' at a lower temperature, effectively establishing a pronounced temperature differential across the cells.

To facilitate the critical electron transfer between the cells, a salt bridge was employed, serving a dual function: it not only preserved the electrolytic equilibrium but also acted as a vital conduit for electron flow, a prerequisite for the success of the experiment. Furthermore, thermocouples were strategically integrated into the electrolytic cells, providing real-time monitoring and meticulous control over the temperature variations during the experimental process.

The electrolyte composition, a critical aspect of the experiment, comprised a carefully formulated mixture of 0.4m/L potassium ferricyanide ($Fe(CN)_6^{4-}$), 0.4m/L potassium ferrocyanide ($Fe(CN)_6^{3-}$), and 1.2m/L KCl. This specific concoction was pivotal in establishing a robust redox reaction system between the cells. Temperature gradients induced around the electrolytic cells markedly influenced the redox dynamics between potassium ferricyanide and ferrocyanide, consequently leading to notable shifts in the electron concentration within the electrolyte. More specifically, at the hot anode, a spontaneous oxidation of $Fe(CN)_6^{4-}$ to $Fe(CN)_6^{3-}$ occurred, leading to an augmentation in the electron density at that locus. In contrast, the cold cathode witnessed a reduction of $Fe(CN)_6^{3-}$ back to $Fe(CN)_6^{4-}$, culminating in a decrement in electron concentration. The strategically positioned KCl within the salt bridge, functioning as an ion transport medium, was critical in maintaining the electrochemical equilibrium across the cells. It facilitated ion mobility while simultaneously inhibiting direct electron exchange, ensuring the electron flux was exclusively confined to the external circuit. Consequently, the potential difference engendered across the cells, resultant from the temperature-driven electron concentration disparity, was measured as the open-circuit voltage (OCV). in Fig.4a, the OCV of the electrode materials displayed a linear correlation with the temperature differences (ΔT) between the electrodes. The slope of the corresponding fitted curve indicated the Seebeck coefficient (Se) of the electrode materials. The determination of the Seebeck coefficient (Se) was predicated on the fundamental principles of the Seebeck effect, where the potential difference (V) is directly proportional to the imposed ΔT, culminating in the formula $Se = \Delta V / \Delta T$. Notably, the Se values for the layered structures, MS and MS-N, showed a significant enhancement. Subsequently, we conducted systematic tests on the output performance of Thermoelectric Converters (TECs) using different electrodes under varying temperature differences (ΔT). As shown in Fig.4b-e, the traditional platinum (Pt) electrode displayed short-circuit currents (Jsc) of 0.21, 0.38, 0.56, and 0.74 mA cm^{-2} under ΔTs of 10, 20, 30, and 40 K, respectively. Upon sequentially replacing the Pt electrode with M+S, MS, and MS-N electrodes, there was a gradual increase in Jsc. Notably, under the MS-N electrode, the maximum Jsc values reached 0.22, 0.43, 0.64, and 0.87 mA cm^{-2} at ΔTs of 10, 20, 30, and 40 K, respectively. This trend aligns with the Faradaic current observed in cyclic voltammetry (CV) analysis, highlighting the significance of electrode material improvements in enhancing thermoelectric conversion efficiency. The maximum output power (Pmax) analysis revealed that at a ΔT of 40 K, the Pmax for the Pt electrode was 10.69 µW cm^{-2}, which increased to 14.11 µW cm^{-2} for the MS-N electrode, as depicted in Fig.4f and g. Compared to the Pt electrode, the Pmax of the MS-N electrode was higher by 31.23%, 29.87%, 34.56%, and 31.99% at ΔTs of 10, 20, 30, and 40 K,

respectively. The MS-N electrode demonstrated a stable power enhancement across different temperature gradients, indicating its significant advantage in facilitating reaction kinetics and a marked increase in current density.

Furthermore, the study also investigated the variations in output current, voltage, and power as a function of load resistance under different ΔT, as illustrated in Fig.4h-j. It was found that the output power P reaches its maximum when load resistance R_L equals the internal resistance R_S of the TEC under any ΔT, in accordance with the formula P = + $R_L/R_S)^2$ (where Voc is the open-circuit voltage).

3.4. Mechanism analysis

The bilayer structure demonstrates significant advantages in enhancing thermoelectric performance, primarily attributed to the unique electronic structures and interactions of the two materials. MXene, such as Ti3C2Tx, being a narrow-bandgap semiconductor, exhibits a bandgap ranging from 0.05 to 0.1 eV and a work function of approximately 3.9 eV. In contrast, SWCNTs display a much wider bandgap of about 2.5 eV and a work function of 4.13 eV[35-37], (Fig.5a). The substantial difference in the bandgaps of these materials leads to the formation of a Schottky barrier at the interface between MXene and SWCNTs. In the field of thermoelectrics, the Schottky barrier is leveraged for carrier selection, allowing high-energy carriers to pass while blocking low-energy ones, thus acting as an energy filter (Fig.5b). This process effectively enhances the Seebeck coefficient and the overall thermoelectric efficiency of the material. In mixed structures, the randomness of the structure may lead to inconsistencies in electronic and thermal transmission paths, subsequently reducing the overall thermoelectric efficiency. In contrast, the layered structure, with its precise control over the arrangement of each material, forms a regular and consistent interface, effectively enhancing the effect of the Schottky barrier, thus optimizing carrier selection and transmission. This orderly structure not only reduces interface scattering but also optimizes carrier transport and lowers thermal conductivity through band engineering. Furthermore, the layered structure also offers improved mechanical and thermal stability due to its optimized interfaces and orderly arrangement. Specifically, in the bilayer structure, the Seebeck coefficient can reach up to -1.59 mV K^{-1}, significantly higher than the -1.49 mV K^{-1} observed in mixed structures. This finding is not only a manifestation of theoretical predictions but also demonstrates the exceptional performance of the MXene and SWCNTs special structure in practical applications. A deep understanding of this mechanism provides crucial guidance for designing and optimizing more efficient thermoelectric materials, suggesting that further enhancements in thermoelectric conversion efficiency and material performance can be achieved by adjusting the proportions and structural arrangements of MXene and SWCNTs.

An in-depth analysis of the nitrogen annealing modification on bilayer electrode materials reveals multifaceted mechanisms of performance enhancement. Initially, the nitrogen annealing modification introduces new electronic levels between the conduction band of MXene and the valence band of SWCNTs, optimizing the electronic structure and reducing defect-induced scattering (Fig.5c). These newly added levels serve as additional channels for electron transport, thereby elevating the material's electron mobility and conductivity. This optimization is crucial for enhancing the overall electrical performance of the electrode. Additionally, empirical data underscores the thermal benefits of nitrogen annealing; for instance, the interface thermal resistance is significantly reduced in the case of MS thin films, from an initial 2.085°C/W down to 1.651°C/W for nitrogen-modified MS-N films. This reduction in thermal resistance indicates a densification of the structure and optimization of the thermal conduction path, with improved interface thermal conduction further enhancing overall thermal conductivity. The enhanced interface interaction reduces carrier scattering at the interface, improving charge transport efficiency. Finally, surface functionalization, achieved through the introduction of nitrogen-containing functional groups, enhances the interaction between the electrode and the electrolyte, thereby boosting electrochemical activity.

3.4. Application research

The nitrogen-annealed MXene and SWCNT bilayer thermoelectric electrodes demonstrate significant potential in the realm of wearable devices. Their distinct flexibility coupled with superior thermoelectric efficiency allows for effortless integration into devices such as smartwatches and health monitoring bands, adeptly converting body heat into

electrical energy. These electrodes, characterized by their slender and pliable attributes, ensure user comfort and diminish reliance on conventional batteries, thereby offering an environmentally sustainable energy solution. Furthermore, these flexible electrodes can be directly employed as thermoelectric materials, broadening their application spectrum. This is especially pertinent in industrial waste heat recovery, where they transform waste heat from mechanical and industrial sources into electrical energy, enhancing overall energy efficiency. In the context of the building industry, they serve to harvest thermal energy originating from sunlight, human activities, or operational equipment, thereby supplying power to minor in-building devices. Additionally, these materials are apt for environmental monitoring instruments, particularly in remote or grid-inaccessible areas, by harnessing environmental temperature differentials to generate electricity. This innovative utilization considerably extends the applicability of thermoelectric materials, contributing to broader energy utilization and advancing sustainable development initiatives.

4. Conclusion

This research presents a groundbreaking advancement in the field of flexible thermoelectric materials with the development of a nitrogen-modified MXene/SWCNT (MS-N) bilayer thin film. The MS-N electrode surpasses traditional Pt electrodes in flexibility and cost-effectiveness, exhibiting exceptional thermoelectric performance, especially in low-temperature heat recovery applications. The nitrogen-doped SWCNT/MXene bilayer thin film is meticulously engineered for thermoelectric applications, showing a significant enhancement in performance compared to conventional Pt electrodes. The MS-N electrode achieves a substantial increase in thermal power output ($14.11 \mu W\ cm^{-2}$) and Seebeck coefficient ($1.61 mV\ K^{-1}$) at a moderate temperature difference of 40°C. This enhancement is primarily attributed to the synergistic effect of nitrogen modification and the bilayer structure, which optimizes the material interface and boosts low-temperature thermoelectric conversion efficiency. This study not only proposes a formidable alternative to traditional electrodes but also highlights the potential for scalable and readily deployable solutions in thermoelectric energy harvesting. The flexibility of the MS-N electrodes makes them particularly suitable for integration into wearable devices, effectively converting body heat into electrical energy and offering an environmentally sustainable energy solution. Moreover, the material demonstrates potential for industrial waste heat recovery, building industry applications, and environmental monitoring, especially in remote areas. This research marks a significant stride in advancing sustainable energy practices, harnessing low-grade thermal energy for practical applications, and paving the way for efficient thermoelectric energy harvesting and sustainable technology development.
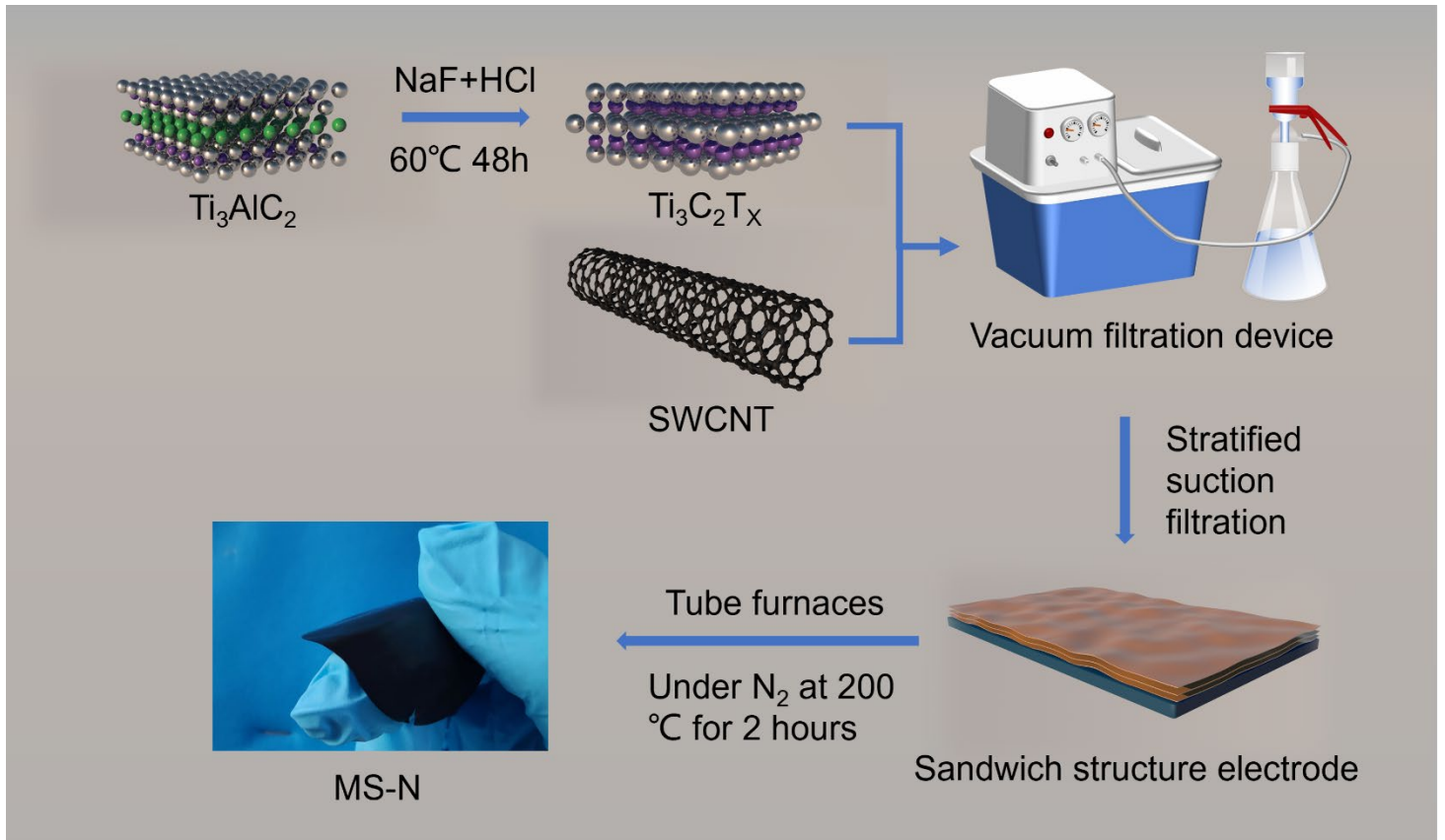
Fig. 1: Schematic representation of flexible thermoelectric electrode materials based on nitrogen-modified SWCNT and MXene bilayer films (MS-N).
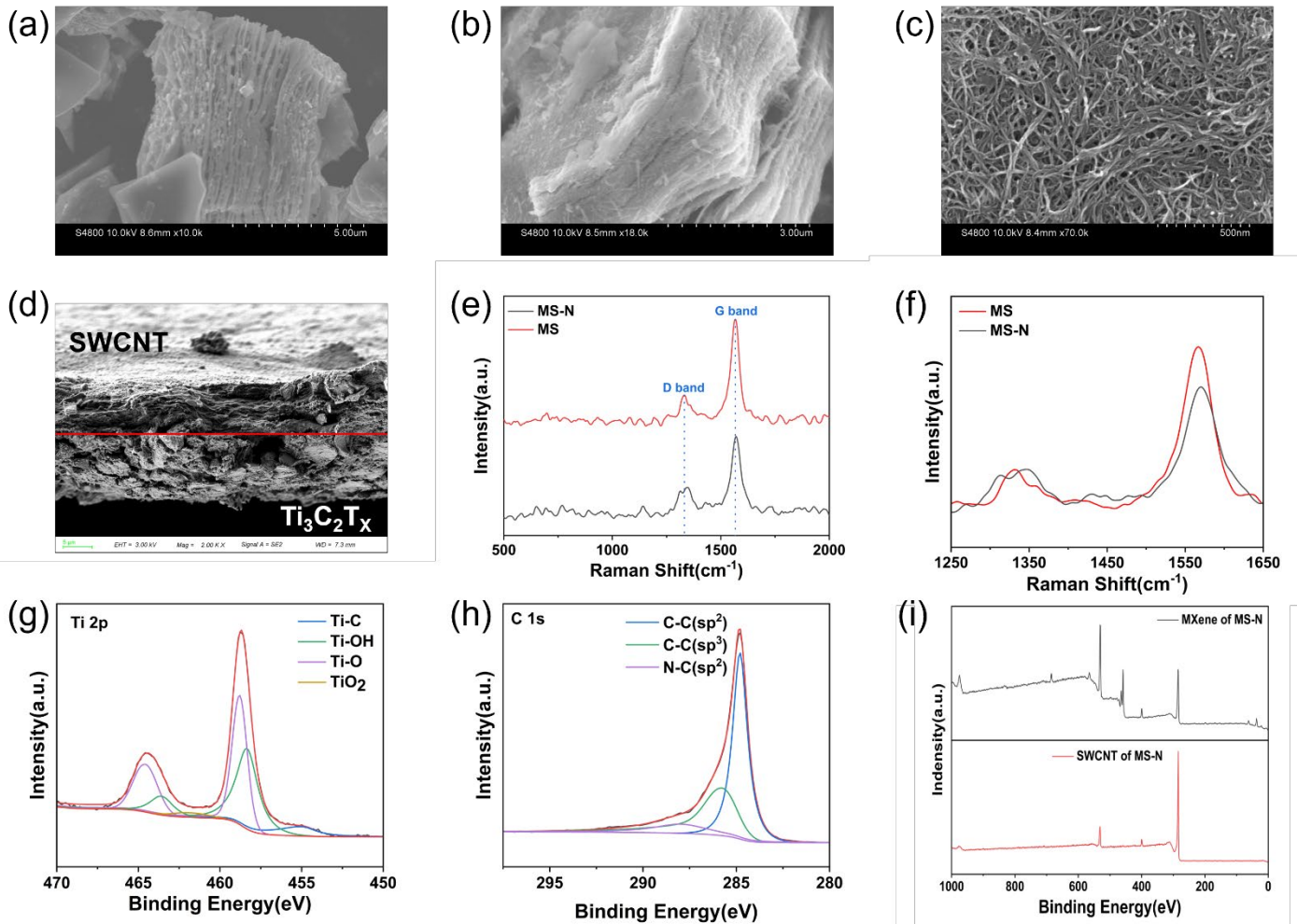
Fig. 2: Surface SEM images of a) Ti3C2Tx, b) MXene side of MS-N film, c) SWCNT side of MS-N film. d) Cross-section of MS-N e) Complete Raman spectral curves of thin film electrodes before and after N2 modification. f) Amplified Raman spectral images of G-band and D-band. XPS spectra of g) Ti 2p on MXene side, h)C 1s on SWCNT side, i) complete of MS-N .
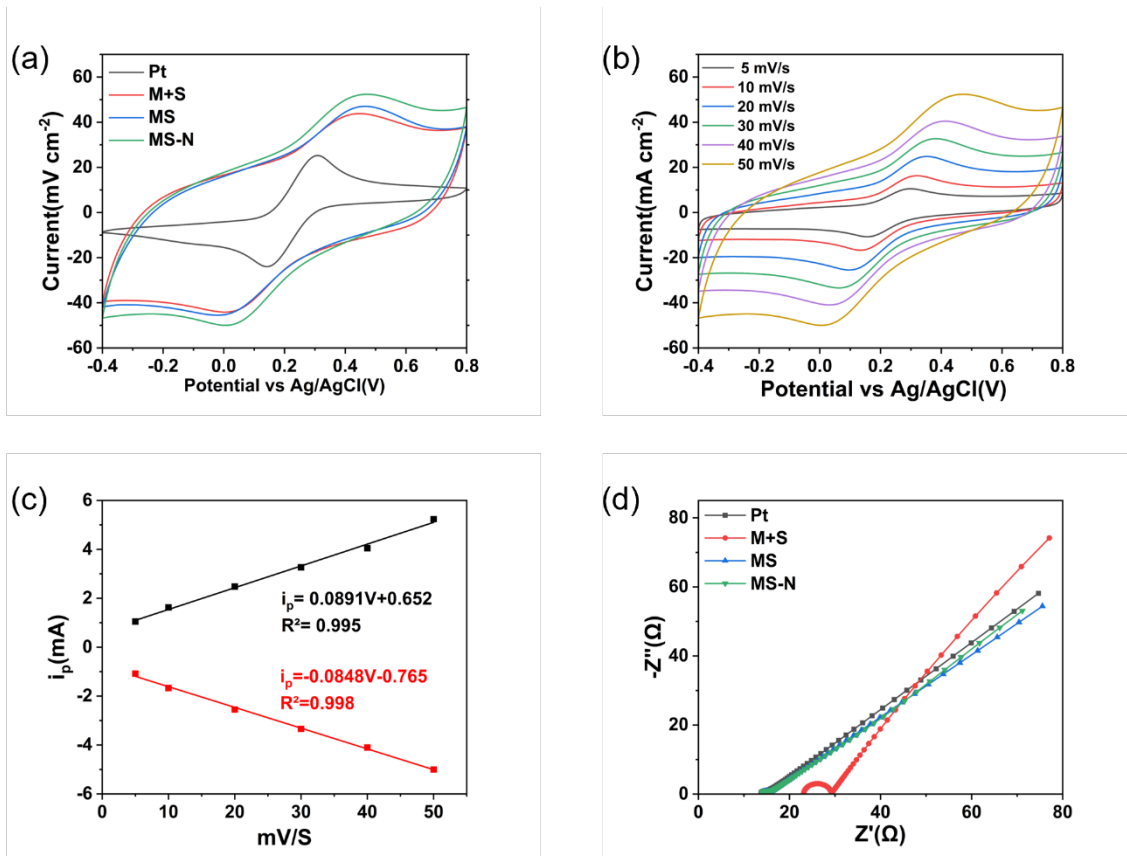
Fig. 3: a) CV curves of Pt, M+S, MS and MS-N in 0.1 M KCl solution containing 5 mM [Fe(CN)6]3-/4-. b) Response of MS-N in 0.1 M KCl solution containing 5 mM [Fe(CN)6]3-/4- solution with sweep rate from 5–50 mV/S. c) Linear plot of peak current versus sweep rate. d) Electrochemical impedance plots of Pt, M+S, MS and MS-N.
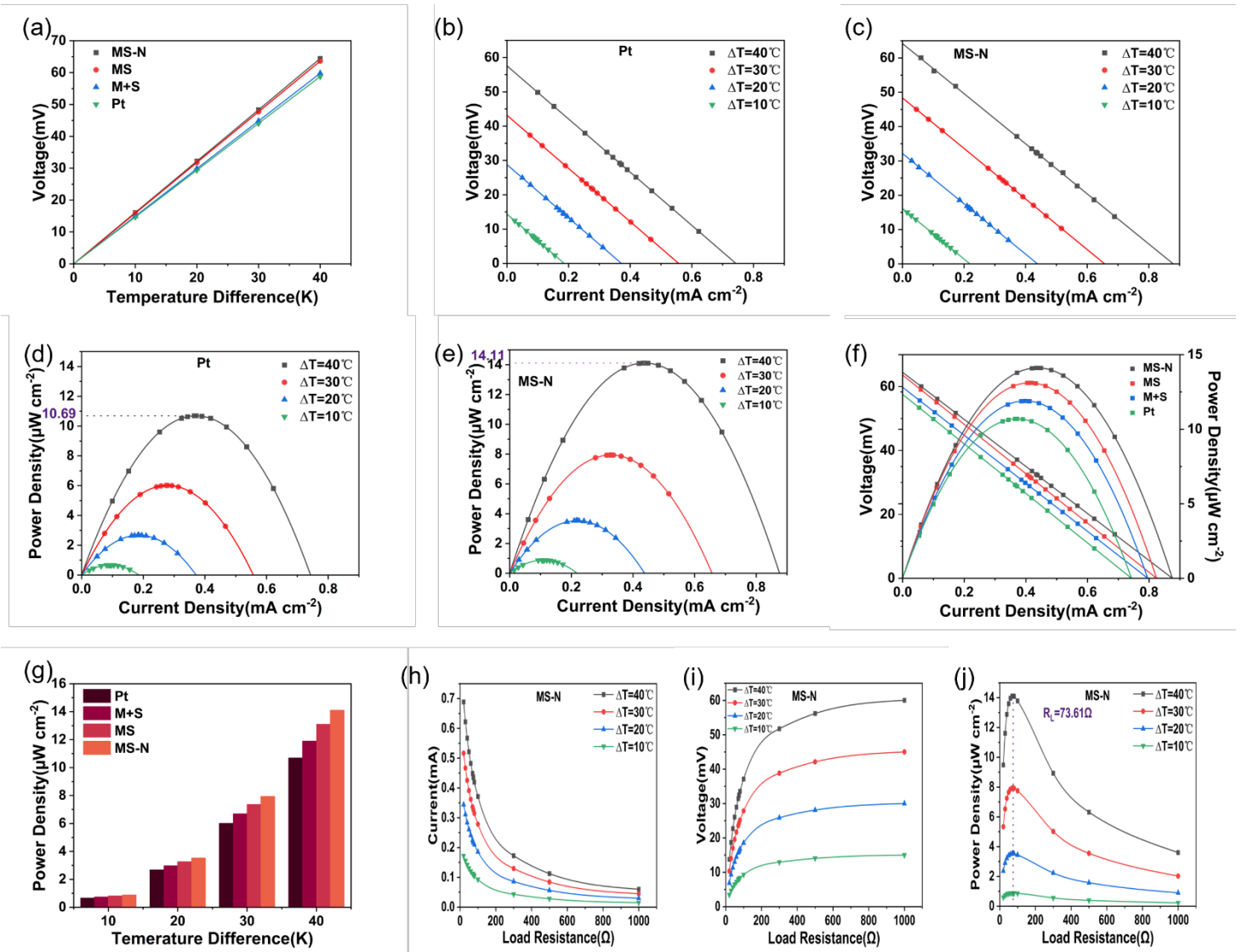
Fig. 4: a) The potential versus temperature difference fitting curves for deriving the Se using various electrodes. b) The output voltage as a function of output current density using Pt electrodes under various temperature differences. c) The output voltage as a function of output current density using MS-N electrodes under various temperature differences. d) The output power density as a function of output current density using Pt electrodes under various temperature differences. e) The output power density as a function of output current density using MS-N electrodes under various temperature differences. f,g) Comparison of output performance for various electrodes under various temperature differences. h) The output current, i) output voltage and j) output power as a function of the load resistance RL using the MS-N electrodes under various temperature differences.
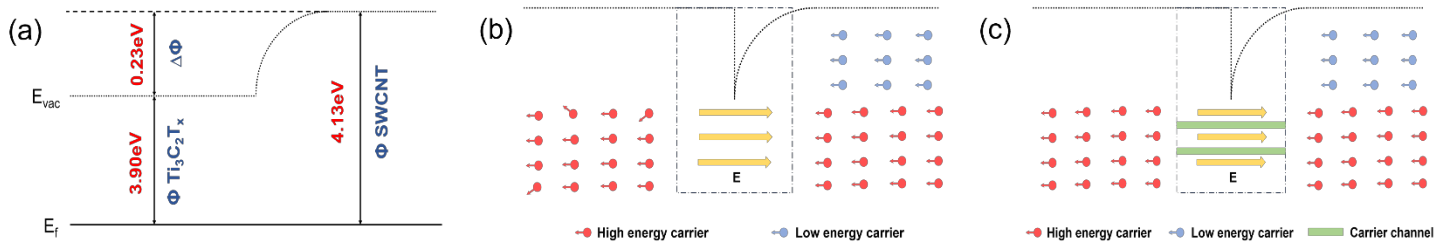
Fig. 5: a) The schematic energy diagrams of MS. b) Schematic diagram of Schottky barrier filtering low energy carriers. c) Schematic of carrier transport after nitrogen modification.

References

[1] Zhang, Jiedong, Chenhui Bai, Zhaosu Wang, Xiao Liu, Xiangyu Li, and Xiaojing Cui, 'Low-Grade Thermal Energy Harvesting and Self-Powered Sensing Based on Thermogalvanic Hydrogels.', *Micromachines*, Jan. 2023, doi: 10.3390/mi14010155.

[2] Sunghoon Hur, Sangtae Kim, Hyun-Soo Kim, Ajeet Kumar, Choah Kwon, Joonchul Shin, Heemin Kang, Tae Hyun Sung, Jungho Ryu, Jeong Min Baik, Hyun-Cheol Song, 'Low-grade waste heat recovery scenarios: Pyroelectric, thermomagnetic, and thermogalvanic thermal energy harvesting', *Nano Energy*, Jun. 2023, doi: 10.1016/j.nanoen.2023.108596.

[3] Burmistrov, Igor, Rita Khanna, Nikolay Gorshkov, Nikolay Kiselev, Denis Artyukhov, Elena Boychenko, Andrey Yudin, Yuri Konyukhov, Maksim Kravchenko, Alexander Gorokhovsky, 'Advances in Thermo-Electrochemical (TEC) Cell Performances for Harvesting Low-Grade Heat Energy: A Review', *Sustainability*, Aug. 2022, doi: 10.3390/su14159483.

[4] Dazhen Huang, Hyunho Kim, Guodong Zou, Xiangming Xu, Yunpei Zhu, Kaleem Ahmad, Zeyad A. Almutairi, Husam N. Alshareef, 'All-MXene thermoelectric nanogenerator', *Mater. Today Energy*, Aug. 2022, doi: 10.1016/j.mtener.2022.101129.

[5] Shi, Xin, Fengmei Guo, Keheng Hou, Guozhen Guan, Lei Lu, Yingjiu Zhang, Jie Xu, and Yuanyuan Shang, 'Highly Flexible All-Solid-State Supercapacitors Based on MXene/CNT Composites', *Energy Fuels*, Jun. 2023, doi: 10.1021/acs.energyfuels.3c01420.

[6] Tingyi, Yan, Zhang Guangyao, Yu Kun, Li Mengjie, Qu Lijun, and Zhang Xueji, 'Smartphone-Based Point-of-Care Testing', *Progress in Chemistry*, vol. 34, no. 4, p. 884, 2022.

[7] Xiuqiang Xie, Meng-Qiang Zhao, Babak Anasori, Kathleen Maleski, Chang E. Ren, Jingwen Li, Bryan W. Byles, Ekaterina Pomerantseva, Guoxiu Wang, Yury Gogotsi, 'Porous heterostructured MXene/carbon nanotube composite paper with high volumetric capacity for sodium-based energy storage devices', *Nano Energy*, Jun. 2016, doi: 10.1016/j.nanoen.2016.06.005.

[8] Yidan, H. E., ZHANG Xiaojuan, YANG Hongjuan, ZHAO Mengmeng, and W. E. N. Bianying, 'Research progress in MXene and its composites for microwave absorption and thermal conduction', *China Plastics*, vol. 36, no. 10, p. 167, 2022.

[9] Du, Yong, Yulu Shi, Qiufeng Meng, and Shirley Z. Shen, 'Preparation and thermoelectric properties of flexible SWCNT/PEDOT:PSS composite film', *Synth. Met.*, Mar. 2020, doi: 10.1016/j.synthmet.2020.116318.

[10] Chuanrui Zhang, Peng-an Zong, Zesheng Ge, Yeming Ge, Jun Zhang, Yujian Rao, Zhenguo Liu, Wei Huang, 'MXene-based wearable thermoelectric respiration sensor', *Nano Energy*, Oct. 2023, doi: 10.1016/j.nanoen.2023.109037.

[11] Li, Tian, Fu Chao, Li Yue-Ming, Fan Xiao-Xing, Wang En-Ge, and Zhao Guo-Rui, 'MAX phase: synthesis, structure and property', *Progress in Physics*, vol. 41, no. 1, p. 39, 2021.

[12] Yan-Zhong PEI, 'Wearable Thermoelectric Cells Based on Gel Electrolytes', *Acta Physico-Chimica Sinica*, vol. 32, no. 11, pp. 2651–2651, 2016.

[13] Ma, Chang, Ming-Guo Ma, Chuanling Si, Xing-Xiang Ji, and Pengbo Wan, 'Flexible MXene-Based Composites for Wearable Devices', *Adv. Funct. Mater.*, vol. 31, no. 22, p. 2009524, May 2021, doi: 10.1002/adfm.202009524.

[14] Zhiwen Wang, Chuanrui Zhang, Jun Zhang, Jia liang, Zhenguo Liu, Fengling Hang, Yuxue Xuan, Xia Wang, Mengran Chen, Shaowen Tang, and Peng-an Zong, 'Construction of an MXene/Organic Superlattice for Flexible Thermoelectric Energy Conversion', *ACS Appl. Energy Mater.*, Sep. 2022, doi: 10.1021/acsaem.2c01855.

[15] Lingling Chu, Chao Xu, Ning Wei, Haibo Wang, Chao Nie, and Liting Deng, 'Performance-enhanced photodetector based on ZnO/MWCNTs/MXene hybrid layer: Enhanced charge transport and hot-electrons injection', *Phys. Lett. A*, Jul. 2023, doi: 10.1016/j.physleta.2023.129036.

[16] Cai, Yong-Zhu, Yong-Sheng Fang, Wen-Qiang Cao, Peng He, and Mao-Sheng Cao, 'MXene-CNT/PANI ternary material with excellent supercapacitive performance driven by synergy', *J. Alloys Compd.*, Feb. 2021, doi: 10.1016/j.jallcom.2021.159159.

[17] Xu Yang, Fengxian Wu, Chunyan Xu, Liying Yang, and Shougen Yin, 'A flexible high-output triboelectric nanogenerator based on MXene/CNT/PEDOT hybrid film for self-powered wearable sensors', *J. Alloys Compd.*, Sep. 2022, doi: 10.1016/j.jallcom.2022.167137.

[18] H. Wang, M. He, and Y. Zhang, 'Carbon nanotube films: preparation and application in flexible electronics', *Acta Phys.-Chim. Sin*, vol. 35, no. 11, pp. 1207–1223, 2019.

[19] Shasha Wei, Yichuan Zhang, Haicai Lv, Liang Deng, and Guangming Chen, 'SWCNT network evolution of PEDOT:PSS/SWCNT composites for thermoelectric application', *Chem. Eng. J.*, Jul. 2021, doi: 10.1016/j.cej.2021.131137.

[20] K. Li, P. Zhang, R. A. Soomro, and B. Xu, 'Alkali-Induced Porous MXene/Carbon Nanotube-Based Film Electrodes for Supercapacitors', *ACS Appl. Nano Mater.*, Feb. 2022, doi: 10.1021/acsanm.2c00109.

[21] An, Cheng Jin, Young Hun Kang, A-Young Lee, Kwang-Suk Jang, Youngjin Jeong, and Song Yun Cho, 'Foldable Thermoelectric Materials: Improvement of the Thermoelectric Performance of Directly Spun CNT Webs by Individual Control of Electrical and Thermal Conductivity', *ACS Appl. Mater. Interfaces*, Aug. 2016, doi: 10.1021/acsami.6b04485.

[22] WANG. Jian and ZHOU. Yuli, 'Research progress of characteristics and applications of two-dimensional nanomaterial MXenes', *Journal of Xihua University (Natural Science Edition)*, vol. 39, no. 3, pp. 76–89, 2020.

[23] Xu, Wenting, Zhao Xu, Yunxia Liang, Lianmei Liu, and Wei Weng, 'Enhanced tensile and electrochemical performance of MXene/CNT hierarchical film', *Nanotechnology*, Jun. 2021, doi: 10.1088/1361-6528/ac04cf.

[24] Dixit, Pragya, Subhra Sourav Jana, and Tanmoy Maiti, 'Enhanced Thermoelectric Performance of Rare-Earth-Free n-Type Oxide Perovskite Composite with Graphene Analogous 2D MXene', *Small*, Feb. 2023, doi: 10.1002/smll.202206710.

[25] Wei, Jiacheng, Dianlun Wu, Chunfa Liu, Fei Zhong, Guibin Cao, Benzhang Li, Chunmei Gao, and Lei Wang., 'Free-standing p-Type SWCNT/MXene composite films with low thermal conductivity and enhanced thermoelectric performance', *Chemical Engineering Journal*, vol. 439, p. 135706, Jul. 2022, doi: 10.1016/j.cej.2022.135706.

[26] X. Guan, W. Feng, X. Wang, R. Venkatesh, and J. Ouyang, 'Significant Enhancement in the Seebeck Coefficient and Power Factor of p-type PEDOT:PSS through the Incorporation of n-type MXene'.

[27] Ding, Wenjun, Peng Liu, Zuzhi Bai, Yeye Wang, Guoqiang Liu, Qinglin Jiang, Fengxing Jiang, Peipei Liu, Congcong Liu, and Jingkun Xu, 'Constructing Layered MXene/CNTs Composite Film with 2D–3D Sandwich Structure for High Thermoelectric Performance', *Adv. Mater. Interfaces*, vol. 7, no. 23, p. 2001340, Dec. 2020, doi: 10.1002/admi.202001340.

[28] Wei, Shouhao, Jiale Ma, Dianlun Wu, Bin Chen, Chunyu Du, Lirong Liang, Yang Huang, Zhenyu Li, Feng Rao, Guangming Chen, and Zhuoxin Liu, 'Constructing Flexible Film Electrode with Porous Layered Structure by MXene/SWCNTs/PANI Ternary Composite for Efficient Low-Grade Thermal Energy Harvest', *Adv Funct Materials*, p. 2209806, Jan. 2023, doi: 10.1002/adfm.202209806.

[29] Yu, Le Ping, Xiao Hong Zhou, Lu Lu, Lyu Xu, and Feng Jun Wang, 'MXene/Carbon Nanotube Hybrids: Synthesis, Structures, Properties, and Applications', *ChemSusChem*, vol. 14, no. 23, pp. 5079–5111, Dec. 2021, doi: 10.1002/cssc.202101614.

[30] Wang, Zhiwen, Mengran Chen, Zhining Cao, Jia Liang, Zhenguo Liu, Yuxue Xuan, Lin Pan, Kafil M. Razeeb, Yifeng Wang, Chunlei Wan, and Peng-an Zong, 'MXene Nanosheet/Organics Superlattice for Flexible Thermoelectrics', *ACS Appl. Nano Mater.*, vol. 5, no. 11, pp. 16872–16883, Nov. 2022, doi: 10.1021/acsanm.2c03813.

[31] M. Sheng, Y. Wang, C. Liu, Y. Xiao, P. Zhu, and Y. Deng, 'Significantly enhanced thermoelectric performance in SWCNT films via carrier tuning for high power generation', *Carbon*, vol. 158, pp. 802–807, Mar. 2020, doi: 10.1016/j.carbon.2019.11.057.

[32] Á. Rodríguez Méndez, L. Medrano Sandonas, A. Dianat, R. Gutierrez, and G. Cuniberti, 'An Atomistic Study of the Thermoelectric Signatures of CNT Peapods', *J. Phys. Chem. C*, Jun. 2021, doi: 10.1021/acs.jpcc.1c02611.

[33] Fan, Bingbing, Siyang Shang, Binzhou Dai, Biao Zhao, Ning Li, Mingqiang Li, Lianji Zhang, Rui Zhang, and Frank Marken, '2D-layered Ti3C2/TiO2 hybrids derived from Ti3C2 MXenes for enhanced electromagnetic wave absorption', *Ceram. Int.*, Jul. 2020, doi: 10.1016/j.ceramint.2020.04.004.

[34] Feng, Aihu, Yun Yu, Yong Wang, Feng Jiang, Yang Yu, Le Mi, and Lixin Song, 'Two-dimensional MXene Ti3C2 produced by exfoliation of Ti3AlC2', *Mater. Des.*, Jan. 2017, doi: 10.1016/j.matdes.2016.10.053.

[35 Ku, Minyue, Congyang Mao, Shuilin Wu, Yufeng Zheng, Zhaoyang Li, Zhenduo Cui, Shengli Zhu, Jie Shen, and Xiangmei Liu, 'Lattice Strain Engineering of Ti3C2 Narrows Band Gap for Realizing Extraordinary Sonocatalytic Bacterial Killing', *ACS Nano*, Jul. 2023, doi: 10.1021/acsnano.3c03134.

[36] Maity, Shilpa, Nayim Sepay, Chiranjit Kulsi, Arpan Kool, Sukhen Das, Dipali Banerjee, and Krishanu Chatterjee, 'Enhancement of Thermoelectric Performance in Oligomeric PEDOT-SWCNT Nanocomposite via Band Gap Tuning', *ChemistrySelect*, Aug. 2018, doi: 10.1002/slct.201801384.

[37] Dass, Devi, and Rakesh Vaid, 'Impact of SWCNT Band Gaps on the Performance of a Ballistic Carbon Nanotube Field Effect Transistors (CNTFETs)', *Journal of Nano- and Electronic Physics*, Jan. 2017, doi: 10.21272/jnep.9(4).04007.